Article

Molecular imaging of mesothelin-expressing ovarian cancer with a human and mouse cross-reactive nanobody

Andrew M Prantner, Catherine Yin, Kalika Kamat, Khushboo Sharma, Andrew C Lowenthal, Peter Bawden Madrid, and Nathalie Scholler

Mol. Pharmaceutics, **Just Accepted Manuscript** • DOI: 10.1021/acs.molpharmaceut.7b00789 • Publication Date (Web): 20 Feb 2018

Molecular imaging of mesothelin-expressing ovarian cancer with a human and mouse cross-reactive nanobody

Andrew M. Prantner[†], Catherine Yin[†], Kalika Kamat[†], Khushboo Sharma[†], Andrew C. Lowenthal[†], Peter B. Madrid[†], and Nathalie Scholler[*†]

† SRI International, Biosciences Division, 333 Ravenswood Ave., Menlo Park, California 94025, United States

*: corresponding author

Nathalie Scholler
333 Ravenswood Ave, room 100-51
Menlo Park, CA 94025

Telephone: 650-859-3248
Fax: 650-859-3153
Email: nathalie.scholler@sri.com

Abstract

Mesothelin is an epithelial marker highly expressed at the cell surface of cancer cells from diverse origins, including ovarian and pancreatic adenocarcinomas and mesotheliomas. Previously, we identified and characterized an anti-mesothelin nanobody (NbG3a) for in vitro diagnostic applications. The main goal of this research was to establish the potential of NbG3a as a molecular imaging agent. Site-specific biotinylated NbG3a (bNbG3a) was bound to streptavidin-conjugated reagents for *in vitro* and *in vivo* assays. Initially, we performed microscale thermophoresis to determine the binding affinity between bNbG3a and human (K_d = 46 ± 8 nM) or mouse (K_d = 4.8 ± 0.4 nM) mesothelin protein. The human and mouse cross-reactivity was confirmed by *in vivo* optical imaging using bNbG3a bound to fluorescent streptavidin. We also localized the binding site of nNBG3a on human mesothelin using overlapping peptide scan. NbG3a recognized an epitope within residues 21-65 of the mature membrane bound form of human mesothelin, which is part of the N-terminal region of mesothelin that is important for interactions between mesothelin on peritoneal cells and CA125 on tumor cells. Next, bNbG3a *in vivo* half-life after intravenous injection in healthy mice was estimated by ELISA assay to be 5.3 ± 1.3 min. In tumor-bearing animals, fluorescent bNbG3a accumulated in a subcutaneous ovarian xenograft (A1847) and in two syngeneic, orthotopic ovarian tumors (intraovary and intraperitoneal ID8) within an hour of intra-venous injection that peaked by 4 hours and persisted up to 48 hours. MRI analysis of bNbG3a-targeted streptavidin-labeled iron oxides showed that the MRI signal intensity decreased one hour after injection for a subcutaneous xenograft model of ovarian cancer for bNbG3a-labeled iron oxides compared to unlabeled iron oxides. The signal intensity differences continued up to the final time point at 24 hours post injection. Finally, *in vivo* immunofluorescence 24 or 48 hours after bNbG3a intravenous injection showed bNbG3a diffuse distribution of both xenograft and syngeneic ovarian tumors, with local areas of high concentration throughout A1847 human tumor. The data

support the use of NbG3a for continued preclinical development and translation to human applications for cancers that overexpress mesothelin.

Keywords: xenograft, syngeneic, orthotopic, in vivo imaging, MRI, epitope, pharmacokinetics, biodistribution.

Introduction

Cancer is the second leading cause of death in the United States and accounts for nearly one of every four deaths, which is estimated to be about 1,650 people per day in 2017.[1] Survival rates can be increased by improved treatments and early detection. One area of active research for increasing survival rates is cancer immunotherapy, which is a biological strategy for treating cancer that uses components from the immune system. In particular, antigen-specific immunotherapy uses molecular recognition of tumor-associated antigens to discriminate between healthy and cancer cells.

Since cancer is a heterogeneous class of diseases, a particular type of cancer can have different subtypes that are characterized by different tumor-associated antigens. For example, a type of ovarian cancer, which is derived from ovarian surface epithelial cells, can be further divided into distinct histological subtypes that have major differences in incidence, malignant potential, response to chemotherapy, and clinical outcome.[2, 3] Each of these epithelial ovarian cancer subtypes has a different molecular phenotype.[2] As a result, effective precision medicine for ovarian cancer requires that the therapy is correctly paired with tumor biomarkers from an individual patient because of the specificity of molecularly-targeted immunotherapies.

Biomarker expression can be quantitatively measured in vivo using molecular imaging. This diagnostic imaging technique broadens the capabilities of available biomedical imaging modalities from anatomic imaging to non-invasive and repetitive characterization of tumor biomarkers located on the cell surface.[4] The phenotype of tumors is determined using biomarker-targeted imaging probes that contain a molecular recognition component responsible for biomarker specificity and a component detectable by the imaging modality. Antibodies have been extensively used as the molecular recognition component for molecular imaging because of their high specificity and affinity. However, a delay of up to one week prior to imaging is needed when using antibodies for imaging because their long circulation time results in a high nonspecific background signal that limits the contrast between tumor and normal tissue.[5] As a

result, antibody engineering has produced numerous different antibody fragments with tunable serum half-lives and rapid tumor penetration that are more suitable for obtaining high contrast images at early time points.[5-7]

Nanobodies (Nbs) or single domain antibodies are recombinant antibody fragments derived from the single antigen binding domain of camelid heavy-chain antibodies.[8] They are being developed for a broad range of applications because Nbs have several useful characteristics compared to conventional antibodies and antibody-derived fragments.[6, 9, 10] One application for Nbs is the targeting component of molecular imaging probes due to the small size and favorable pharmacokinetics of nanobodies combined with high solubility, convex paratope, and stability to thermal and chemical denaturation. Nanobodies have been used as targeted molecular imaging probes to detect numerous extracellular tumor biomarkers that include epidermal growth factor receptor, human epidermal growth factor receptor 2, and carcinoembryonic antigen.[11-14]

Mesothelin is an extracellular, glycosylphosphatidylinositol-anchored glycoprotein that is overexpressed in approximately 30% of human cancers.[15] The limited expression of mesothelin in normal tissues makes it an appealing biomarker for preclinical development and clinical application of mesothelin-targeted immunotherapies.[16] In the United States, there are more than 40 clinical trials (www.clinicaltrials.gov) in various stages that involve mesothelin expressing cancers, which illustrates the importance of mesothelin for targeted therapies.[16] These strategies use a chimeric monoclonal antibody (MORAb-009/amatuximab), an immunotoxin (SS1P), a next generation immunotoxin with reduced immunogenicity (RG7787/LMB-100), antibody drug conjugates (anetumab ravtansine or BMS-986148), chimeric antigen receptor T-cells, or vaccination using attenuated Listeria monocytogenes that express human mesothelin. The success of these strategies depends on diagnostic identification of patients, with mesothelin positive tumors, who are most likely to respond to the mesothelin targeted therapies.

We previously isolated and characterized a high affinity anti-mesothelin Nb, G3a, with an apparent dissociation constant determined by flow cytometry (K_D = 15 nM) similar to the commercial antibody K1.[17] Native and denatured mesothelin was detected using NbG3a in several *in vitro* diagnostic applications that include flow cytometry, western blotting, immunofluorescence, and optical imaging. Here we extended the characterization of NbG3a binding affinity by microscale thermophoresis and we localized the epitope recognized by NbG3a using an overlapping 25-mer oligopeptide array. Then, the pharmacokinetics and tumor distribution of NbG3a were determined for comparison to other published nanobodies and as a baseline for future studies using NbG3a as an immunoPET probe or exploring half-life extension strategies for NbG3a. Finally, we evaluated the potential of site-specifically biotinylated NbG3a (bNbG3a) as a mesothelin-targeted preclinical molecular imaging probe for human and mouse mesothelin using magnetic resonance imaging (MRI) and fluorescence optical imaging in mouse models of ovarian cancer. Two important results from these studies are: (i) NbG3a can bind to human and mouse mesothelin *in vitro* and (ii) NbG3a cross-reactivity between human and mouse mesothelin is preserved *in vivo*, which can be used to highlight potential unintended antigen-specific on-target, off-tumor effects of mesothelin-targeted therapies.

Experimental Section

Biotinylation, expression and purification of recombinant antibodies. Site-specific, biotinylated antibody fragments were generated biosynthetically by yeast using an established protocol.[18] Briefly, NbG3a [17] was fused to an N-terminal biotin-accepting site that is biotinylated by a biotin ligase during secretion by diploid yeast in the presence of galactose. Secreted recombinant antibodies expressed a HIS tag that permits isolation directly from yeast culture supernatant using HIS-Select Nickel Affinity Gel (Sigma-Aldrich) [19]

Determining NbG3a dissociation constants using microscale thermophoresis. The biotinylated G3a nanobody was fluorescently labeled at its C-terminus 6-His tag using a Ni-NTA-Dye with fluorescent excitation in the 650 nm region. A solution of bNbG3a (100 µL of a 200 nM solution) was mixed with 100 µL of the 100nM Ni-NTA-647 dye (Nanotemper) and incubated for 30 minutes at room temperature. The labeled protein was then centrifuged for 10 minutes at 15,000 × g. Recombinant human and mouse mesothelin were titrated over a range from 30 pM to 1 µM concentration while keeping the concentration bNbG3a-dye conjugate fixed at 5 nM and allowed to sit for 10 minutes at room temperature before microscale thermophoresis analysis. bNbG3a and mesothelin were diluted into microscale thermophoresis buffer with Tween-20 and BSA (50 mM Tris-HCl pH 7.4, 150 mM NaCl, 10 mM MgCl2, 0.05 % Tween-20, .4%BSA). MST analysis was performed in triplicate for human and mouse mesothelin under default conditions (excitation power 20%, MST Power 40%).

Peptide mapping ELISA. A library of 25-mer peptides with a five amino acid overlap was synthesized (Genscript, USA Inc.) based on the mesothelin sequence reported in the National Institute of Allergy and Infectious Disease Immune Epitope Database (www.iedb.org/assay/2095150). Stock solutions (10 mg/mL) of each peptide were made by dissolving the peptides in PBS. The peptides (50 µL) at a working concentration of 10 µg/mL in bicarbonate buffer were adsorbed in duplicate to wells of a 96-well microtiter plate (Nunc® CovaLink™) overnight at 4 ℃. Wells were blocked with 100 µl of 1% BSA in PBST (0.05% Tween-20 in PBS) for 1h at 37˚C, washed twice with 200 µl of PBST and incubated with antibody fragments (50 µL,10 µg/mL) in 3% BSA PBST for 1h at 37˚C. After 3 washes with 200 µL PBST, antibody binding to peptides was detected by incubation with 50 µl of streptavidin-conjugated to horseradish peroxidase diluted 1:500 in 3% BSA in PBST for 30 min at 37˚C. Color development was performed after three PBST washes with TMB peroxidase substrate (50 µL, Kirkegaard and Perry Laboratories). The colorometric reaction was stopped with 50 µL of 1M H_2SO_4 prior to reading the absorbance at 450 nm

Blood clearance. Wild type C57Bl/6 female mice (n = 15) were injected retro-orbitally with bNbG3a (30 µg in 100 µL of PBS per mouse), bNbG3a coupled 1:1 to dialyzed IRDye 680RD streptavidin (LI-COR Biosciences) (30 µg of each in 100 µL of PBS per mouse), or dialyzed IRDye 680RD streptavidin only (30 µg in 100 µL of PBS per mouse). Blood was collected from five groups each consisting of three mice at 2 time points per mouse. The first sample was obtained retro-orbitally from the contralateral eye and the second sample was a terminal cardiopuncture. This collection schemed allowed 10 time points (1, 5, 10, 15, 20, 30, 40, 50, 60, and 90 min) to be collected in triplicate. Sera were separated from blood by centrifugation and stored at -20˚C until assay. An ELISA was used to determine the serum concentration of bNbG3a.

ELISA assay for bNbG3a pharmacokinetic studies. Briefly, Nunc Maxisorb plates were coated with 50µL of 1 µg/mL anti-Flag antibody (Ab) in bicarbonate buffer over night at 4˚C. After blocking with Superblock according to the manufacturer instruction, wells were incubated with serum (4 fold dilution) in PBST supplemented with 1% BSA fraction V (PBST-BSA) for 1hr at room temperature (RT) with gentle rotation. Wells were washed three times with PBST and Ab-captured nanobody was labeled with 1 µg/mL HRP-conjugated anti-V5 antibody (Ab) in PBST-BSA for 30 min at RT. Color development was performed as described for peptide mapping.The bNbG3a concentrations as a function of time after injection were used to estimate the blood half-life for bNbG3a using a one phase decay equation in GraphPad Prism..

Cell culture. Human ovarian cancer cell lines (A1847 and C30) were grown in RPMI-1640 and a mouse ovarian cancer cell line expressing luciferase (Luc-ID8) was grown in DMEM. All media were supplemented with 10% fetal bovine serum (Sigma-Aldrich) and 1% penicillin-streptomycin (Gemini Bio Products). Cells were grown in a humidified incubator at 37 ℃ with 5% carbon dioxide.

Mouse models. Syngeneic, orthotopic mouse models were established by injecting Luc-ID8 cells[20] into the ovary (5 million cells in 10 µL PBS)[21] or the peritoneal cavity (5 million cells in

100 µL PBS) of 8 -12 week old female C57BL/6 mice (Charles River). Xenograft models were established by injecting 8 -12 week old female NOD scid gamma mice (NSG, Charles River) subcutaneously with A1847 cells (5 million cells in 100 uL PBS). Tumors were allowed to grow for 7 weeks (A1847) or 8 weeks (Luc-ID8) prior to imaging.

***In vivo* MRI.** Mesothelin-targeted nanoparticles for in vivo imaging were prepared by incubating streptavidin-coated paramagnetic nanoparticles (50 µL, Nanocs) with 30 µg of bNb A1 for 30 minutes at 4 ℃. Two mice were imaged 7 weeks after subcutaneous implantation of A1847 cells. Coronal images of mice were collected on a 16 cm horizontal bore Bruker PharmaScan 70/16 using Paravision 6.0.1 software with a 40 mm coil before injection and at the indicated time points after retro-orbital injection of targeted or untargeted paramagnetic nanoparticles. Images were collected using a T2 TurboRare sequence with a 25 × 25 mm FOV, slice thickness = 0.5 mm, TR = 2400 ms, 20 slices, TE = 37 ms, RARE factor = 4, and an effective echo time = 18.5 ms. For each slice containing tumor, the signal intensity of the tumor was normalized to the signal intensity of the muscle using a region-of-interest analysis in ImageJ.

***In vivo* optical imaging.** IRDye 680RD streptavidin (LI-COR Biosciences) was dialyzed to remove preservatives and then incubated with 30 µg of nanobody at a 1:1 ratio for 30 minutes on ice. The mix (80 – 120 µL) was then retro-orbitally injected into three mice with intraovary Luc-ID8 tumors and two mice with intraperitoneal Luc-ID8 tumors. Two tumor-bearing mice, one for each ovarian cancer model, were injected with untargeted streptavidin as controls. Mice were imaged prior to the injections and at the indicated time points after injection. Luc-ID8 tumors were imaged by bioluminescence to determine tumor burden following the last fluorescent time point. For bioluminescence images, mice received an intraperitoneal injection (200 µL of a 15 mg/mL solution) of D-luciferin (PerkinElmer). Fluorescence and bioluminescence imaging was performed on an In Vivo Imaging System (IVIS, PerkinElmer).

Living Image software was used to display data as radiance (bioluminescence) or radiant efficiency (fluorescence) and data analysis.

Immunofluorescence for bNbG3a biodistribution studies. C57/Bl6 female mice bearing intraovary ID8 tumor (n=2) and female NSG mice (n = 2) bearing an A1847 subcutaneous tumor were retro-orbitally injected with 30 µg of bNbG3a and sacrificed 24 hours or 48 hours after the injection. Organs (spleen, liver, kidneys, lungs and ovaries) and ID8 ovarian tumors or A1847 subcutaneous tumors were immediately fixed in formalin and then stored in 70% ethanol until sectioning. Slides were heated in an oven to 60˚C for 20 min. Slides were deparaffinized in xylene for 10 minutes and rehydrated through a graded ethanol series. Antigen retrieval was carried out by heating the slides in citrate buffer for 10 min at 93 ˚C. Slides were allowed to cool down for 25 min before incubation with Qdot 800 Streptavidin Conjugate (ThermoFisher,1:50 dilution in PBS) was carried out for 1 hour at room temperature in the dark. Slides were then washed 3 times for 5 minutes in PBS with 0.05% Tween-20. Counterstaining was carried out with DAPI at 1:10000 for 15 minutes in the dark. Slides were washed twice for 2 minutes in PBS and FluorSave Reagent (Calbiochem) was used to mount coverslips onto the slides. Fluorescent images (ex:420/40, em: 800/50) were collected with a 20× objective on a Nikon TE2000U 80i.

Mouse Ethics. All animal studies and procedures were conducted under a protocol approved by the SRI International Institutional Animal Care and Use Committee. SRI International maintains a centralized animal care and use program registered with the U.S. Department of Agriculture (USDA), accredited by the Association for Assessment and Accreditation of Laboratory Animal Care International (AAALAC) and has an Assurance on file with the Office of Laboratory Animal Welfare (OLAW).

Statistical Analysis and Error Propagation. All quantitative data are presented as mean ± standard deviation. Statistical analysis was performed with a two tailed Student's *t*-test with two samples assuming unequal variance. P-values less than 0.05 were considered

statistically significant. The uncertainty of derived values were calculated by propagating the experimentally determined uncertainties using the general partial derivative formula. In this case, the uncertainty is equal to the square root of the squared sums of the uncertainty in the variables multiplied by the partial derivative with respect to that variable.

Results

Microscale thermophoresis quantitation of bNbG3a binding to human and mouse mesothelin proteins. The G3a nanobody has been evaluated for affinity towards recombinant mouse and human mesothelin proteins using a microscale thermophoresis (MST) binding assay.[22] The principle of the assay is based on the measurement of macromolecules moving through a temperature gradient (thermophoresis) after titration of an interacting ligand. The binding interaction results in changes to the hydration shell of the biomolecules, giving rise to a shift in thermophoresis rates that can be related to the equilibrium binding affinity (K_d). The biotinylated G3a nanobody was fluorescently labeled at its C-terminus 6-His tag using a Ni-NTA-Dye with fluorescent excitation in the 650 nm region. This assay shows binding affinities of 4.8 ± 0.4 and 46 ± 8 nM against mouse and human mesothelin proteins respectively (**Fig. 1**). These strong binding interactions against both mouse and human mesothelin proteins demonstrate the ability of bNbG3a to target mesothelin and this MST binding assay can be used to characterize other anti-mesothelin nanobody constructs for additional optimization.

Epitope mapping. The epitope of nanobody bNbG3a was localized using an overlapping 25-mer oligopeptide array starting from amino acid 296 in the human mesothelin precursor protein (**Fig. S1**), which is the N-terminal residue of membrane-bound mesothelin. Peptides 2, 3, and 9 were recognized by bNbG3a (**Fig. 2**). These peptides correspond to amino acids 21-45, 41-65, and 161-185 of the mature, membrane-bound form of mesothelin.

Pharmacokinetic studies of bNbG3a and bNbG3a coupled to labeled streptavidin. A sandwich test ELISA assay was used to determine the concentration of bNbG3a in serum at

10 time points after an intravenous injection of 30 µg of bNbG3a. The bNbG3a blood half-life (5.3 ± 1.3 min) was estimated with a one phase decay equation because the data did not support a more complex model (**Fig. 3A**). Next, we coupled bNbG3a to fluorescent streptavidin (IRDye 680RD streptavidin); sera were harvested at various time points after injections and analyzed for fluorescence by In Vivo Imaging System (IVIS, PerkinElmer) and Living Image software (**Fig. S2)**. The half-life of bNbG3a coupled to IRDye 680RD streptavidin was estimated at 2.2 hrs (**Fig. 3B**, orange line).

Biodistribution. The biodistribution and tumor distribution of bNbG3a was determined by immunofluorescence 24 hours (A1847) or 48 hours (Luc-ID8) after an intravascular injection of the single domain antibody fragment (**Fig. 4**). The A1847 xenograft (**Fig. 4a**) and the ID8 syngeneic tumors (**Fig. 4b**) showed a diffuse distribution of bNbG3a throughout the tumor with local areas of high bNbG3a accumulation. At this time point, there was no signal from the liver, spleen, kidneys, or lungs (**Fig. S3**).

MRI detection of bNbG3a binding in a subcutaneous human ovarian cancer xenograft. Mesothelin-positive human ovarian cancer cells (A1847) were injected on the flank of NSG mice to generate subcutaneous tumors. Mice were injected with streptavidin-coated iron oxide nanoparticles that were either untargeted or targeted to mesothelin using bNbG3a. Longitudinal MRI data was collected after the injection and analyzed for antigen-specific tumor accumulation of bNbG3a-targeted iron oxide nanoparticles. Qualitative images before the injection (**Fig. 5A**) and four hours after the injection (**Fig. 5B**) indicate that the signal intensity was decreased, which corresponds to iron oxide nanoparticle accumulation, in the tumor after injection of bNbG3a-targeted iron oxide nanoparticles compared to untargeted iron oxide nanoparticles. A region of interest analysis was used to calculate the normalized signal intensity by dividing the signal intensity within the tumor by the muscle signal intensity for both the untargeted and bNbG3a-targeted iron oxide nanoparticles (**Fig. 5C**). The signal intensity difference between untargeted and antigen-specific iron oxide nanoparticles was statistically

significant ($p < 0.05$) from the one-hour time point to the final time point at 24 hours post injection.

Optical detection of bNbG3a binding in three mouse models of ovarian cancer. Three mouse models of ovarian cancer were used for longitudinal fluorescence monitoring of bNbG3a tumor accumulation. In addition to a subcutaneous xenograft model (A1847), two syngeneic, orthotopic models of ovarian cancer were induced by intravoary or intraperitoneal injection of mesothelin-positive Luc-ID8 cells. Binding of bNbG3a to tumors expressing mesothelin was detected with IRDye 680RD streptavidin that was functionalized with bNbG3a (**Fig. 6**). The fluorescent bNbG3a-streptavidin increases the blood circulation time compared to bNbG3a (**Fig. 3B** and **Fig. S2**), and does not have the potential for high contrast imaging at early time points. However, the construct is suitable for noninvasive preclinical imaging to characterize antigen-specific accumulation. Tumor burden in the syngeneic Luc-ID8 tumors was imaged by bioluminescence after collecting the last fluorescent image for each model (**Fig. S4**). Uptake kinetics differed between the mouse models (**Fig. S5**), but all mice showed tumor fluorescence by one hour after an intravascular injection. The signal peaked around the four-hour time point and remained until at least 48 hours post injection.

Discussion

Mesothelin is a solid tumor biomarker that is actively being investigated as an immunotherapy target in both preclinical research and clinical trials.[16, 23, 24] In addition, mesothelin is a target of molecular imaging probes that are designed to guide individualized antibody-based treatments by evaluating tumor uptake, response to treatment, and whole-body distribution in primary tumors and metastases.[25-28]

We previously generated and characterized the in vitro applications of an anti-mesothelin nanobody (NbG3a) obtained by phage-display from a llama immunized with recombinant human mesothelin.[17] It is usually difficult to obtain a single domain antibodies that

cross reacts with human and mouse homologs without special immunization and selection procedures because nanobodies preferentially recognize conformational epitopes.[29] But as shown in Figure 1, we confirmed that NbG3a recognized both human and mouse mesothelin despite a 58% sequence similarity between the human mesothelin peptide array sequence and mouse mesothelin (Fig.S1). The binding affinity to human (K_d = 46 ± 8 nM) and mouse (K_d = 4.8 ± 0.4 nM) mesothlin was determined using microscale thermophoresis, which quantitatively measures the shift in thermophoresis rates to determine the equilibrium binding affinity. The human and mouse cross-reactivity of NbG3a will allow the preclinical evaluation of potential on-target, off-tumor binding and facilitate translation of preclinical studies to clinical molecular imaging and therapeutic applications.

We also wanted to localize the epitope and further evaluate NbG3a as a potential molecular imaging probe for mesothelin positive tumors. The epitope for NbG3a was localized using an overlapping peptide library based on the human mesothelin sequence. There was specific binding of NbG3a (Fig. 2) to peptides that covered amino acid residues 21 – 65 (peptide_02 and peptide_03) and 161-185 (peptide_09) from the mature, membrane-bound form of human mesothelin. Binding to the region containing residues 21 – 65 is particularly interesting because this region contains the discontinuous epitope for MORAb-009 (Fig. S1) and is involved in the interaction between mesothelin on peritoneal cells and CA125 on tumor cells.[30, 31] Therefore, NbG3a has potential as a therapeutic to disrupt the CA125-mesothelin interaction and improve the survival of ovarian cancer patients by preventing or treating peritoneal metastasis.[18, 30, 32, 33] The relevance of NbG3a binding to a peptide containing the amino acid residues 161-185 requires additional epitope mapping and structure-function studies because the N-terminal fragment (amino acid residues 7 – 64)[31] is the only experimental three-dimensional structure for mesothelin. There is a homology model of full-length mesothelin.[34] However, the experimentally determined structure of the N-terminal fragment had large deviations compared to the homology model,[31] so any comparisions to the homology model

would be highly speculative. Additional structure-function studies could include a solution-phase peptide mapping experiment to address potential artifacts from the solid-phase ELISA due to the convex paratope of the nanobody or hydrogen-deuterium exchange by mass spectrometry or NMR to define the interacting amino acid residues.

The high affinity, small size, and rapid kidney clearance of nanobodies is important for their use as diagnostics and radioimmunotherapeutics to minimize radiation doses to the bone marrow. The short in vivo half-life for nanobodies is a benefit for molecular imaging because the unbound, nonspecific signal is removed and high contrast images can be collected within several hours of injection.[13, 35-37] The half-life for NbG3a was estimated as 5.3 ± 1.3 min (Fig. 3A), which is consistent with other nanobodies.[13, 35, 36, 38] The blood lifetime of NbG3a allows comparison of our construct with other published studies and as a baseline for comparison with potential NbG3a site-specifically labeled with an FDA approved fluorophore (indocyanine green), a radiolabel chelator, or a modified construct incorporating a half-life extension strategy. In addition and as a proof of concept, we showed that coupling bNbG3a to labeled streptavidin can increase the blood clearance half time to approximately two hours (Fig. 3B) compared to about 5 minutes for bNbG3a, which is of interest for various therapeutic applications. Despite the rapid clearance, the NbG3a distributed throughout an A1847 human xenograft tumor and ID8 syngeneic tumor with areas of high accumulation and did not accumulate in the kidney, liver, spleen, or lungs (Fig. 4 and S3). Inhomogenous tumor antigen expression can contribute to the staining pattern. However, non-uniform uptake of systemically administered antibodies or antibody fragments is generally observed in solid tumors.[39, 40] The heterogeneous staining within the tumor can be expected based on physiological barriers that include heterogeneous vascular density, elevated interstitial pressure of solid tumors, and the binding site barrier, which describes the differential binding of antibody to antigen immediately outside of a vascular wall or in the periphery of a tumor.[41-43]

The cross-reactivity between human and mouse proteins is an important variable to consider because antibodies raised against a specific human antigen often do not cross-react with nonhuman versions of that antigen. As an example, a high affinity antibody fragment was identified that reacted with the human TNF-α converting enzyme ectodomain but lacked recognition of the mouse ectodomain despite a 95.6% amino acid homology.[44] In addition, trastuzumab (Herceptin), a humanized monoclonal antibody directed against an epitope in the HER2 receptor ectodomain used animal models to validate HER2 as a potential monoclonal antibody target. The principle shortcoming of animal modeling in the development of trastuzumab was determined to be the lack of cross reactivity of trastuzumab to non-human HER2.[45] Since trastuzumab did not cross react with the murine protein, it was not possible to anticipate toxicities in human studies like cardiac dysfunction.

We chose to evaluate the potential of NbG3a to recognize mesothelin in vivo using MRI and fluorescence imaging. Biotinylated NbG3a was attached to either fluorescent-labeled streptavidin or streptavidin-labeled iron oxides. These constructs are larger than NbG3a and are not capable of demonstrating the rapid high-contrast imaging possible with nanobodies. However, they are suitable for a preclinical study to non-invasively image tumor accumulation of the targeted constructs. The targeted iron oxides are commercial and not optimized for in vivo applications, but there is a qualitative reduction in signal intensity within the subcutaneous A1847 tumor when comparing T_2-weighted MRI images collected prior to injection and four hours after injection (Fig. 5A and 5B). The signal intensity was compared between untargeted and NbG3a-targeted iron oxides. Threre was a statistically significant ($p < 0.05$) reduction in the signal intensity of the tumor, which was normalized by the signal intensity of the muscle, for all time points (Fig. S4). In vivo fluorescence imaging of a human A1847 xenograft or syngenic, orthotopic (intraovary and intraperitoneal) Luc-ID8 mouse models confirmed the human and mouse cross-reactivity of NbG3a (Fig. 6). In addition, there was minimal accumulation in animals injected with untargeted, fluorescent streptavidin (Fig. S5)

The streptavidin-biotin system was chosen to evaluate the potential for NbG3a to target mesothelin expressing tumors in vivo because of the strong binding affinity. The size of the constructs and the immunogenicity of streptavidin precludes direct human translation of the streptavidin-biotin system used here for preclinical evaluation of NbG3a. However, future experiments are being designed to use NbG3a that has been bioconjugated site-specifically to a radiolabel chelator as an immunoPET tracer because the increased sensitivity of PET compared to MRI or optical imaging has the potential to increase the survival rates of patients through early detection of ovarian cancer.

Conclusion

The anti-mesothelin nanobody G3a detects both human and mouse mesothelin using fluorescence imaging or MRI. The human and mouse cross-reactivity allows any potential on-target, off-tumor side effects to be evaluated at the preclinical stage, which is frequently unavailable information for species-specific antibodies and antibody fragments. These results support the continued preclinical development of NbG3a and translation to human imaging and therapeutic applications in cancers that overexpress mesothelin. The streptavidin and iron oxide imaging probes used for noninvasive detection of mesothelin expressing tumors are limited to preclinical applications. However, potential clinical applications for NbG3a are as a component of therapeutic molecules (bispecific antibody fragments or immunotoxins) or as a immunoPET imaging probe to detect mesothelin-expressing cancer in the clinic at an early, localized stage, which is essential for improving patient survival rates.

Acknowledgements

This work was supported by internal funding from SRI International. We thank NCI Prevent for providing the mesothelin peptides used for epitope mapping.

Supporting Information

The Supporting Information is available free of charge on the ACS Publications website at DOI:

Sequences of human mesothelin peptides, Fluorescence imaging of sera from mice injected with bNbG3a coupled to IRDye 680RD streptavidin or with IRDye 680RD streptavidin only, biodistribution immunofluorescence, bioluminescence images of orthotopic Luc-ID8 tumors, tumor accumulation kinetics of fluorescent bNbG3a, fluorescence images of control mice injected with fluorescent streptavidin.

References

1. Siegel, R. L.; Miller, K. D.; Jemal, A. Cancer Statistics, 2017. *CA Cancer J Clin* **2017,** *67*, (1), 7-30.
2. Banerjee, S.; Kaye, S. B. New strategies in the treatment of ovarian cancer: current clinical perspectives and future potential. *Clin Cancer Res* **2013,** *19*, (5), 961-8.
3. Karst, A. M.; Drapkin, R. Ovarian cancer pathogenesis: a model in evolution. *J Oncol* **2010,** *2010*, 932371.
4. Massoud, T. F.; Gambhir, S. S. Molecular imaging in living subjects: seeing fundamental biological processes in a new light. *Genes Dev* **2003,** *17*, (5), 545-80.
5. Knowles, S. M.; Wu, A. M. Advances in immuno-positron emission tomography: antibodies for molecular imaging in oncology. *J Clin Oncol* **2012,** *30*, (31), 3884-92.
6. Holliger, P.; Hudson, P. J. Engineered antibody fragments and the rise of single domains. *Nat Biotechnol* **2005,** *23*, (9), 1126-36.
7. Kenanova, V.; Olafsen, T.; Crow, D. M.; Sundaresan, G.; Subbarayan, M.; Carter, N. H.; Ikle, D. N.; Yazaki, P. J.; Chatziioannou, A. F.; Gambhir, S. S.; Williams, L. E.; Shively, J. E.; Colcher, D.; Raubitschek, A. A.; Wu, A. M. Tailoring the pharmacokinetics and positron emission tomography imaging properties of anti-carcinoembryonic antigen single-chain Fv-Fc antibody fragments. *Cancer Res* **2005,** *65*, (2), 622-31.
8. Muyldermans, S. Nanobodies: natural single-domain antibodies. *Annu Rev Biochem* **2013,** *82*, 775-97.
9. Huang, L.; Muyldermans, S.; Saerens, D. Nanobodies(R): proficient tools in diagnostics. *Expert Rev Mol Diagn* **2010,** *10*, (6), 777-85.
10. Saerens, D.; Ghassabeh, G. H.; Muyldermans, S. Single-domain antibodies as building blocks for novel therapeutics. *Curr Opin Pharmacol* **2008,** *8*, (5), 600-8.

11. Chakravarty, R.; Goel, S.; Cai, W. Nanobody: the "magic bullet" for molecular imaging? *Theranostics* **2014,** *4*, (4), 386-98.
12. Keyaerts, M.; Xavier, C.; Heemskerk, J.; Devoogdt, N.; Everaert, H.; Ackaert, C.; Vanhoeij, M.; Duhoux, F. P.; Gevaert, T.; Simon, P.; Schallier, D.; Fontaine, C.; Vaneycken, I.; Vanhove, C.; De Greve, J.; Lamote, J.; Caveliers, V.; Lahoutte, T. Phase I Study of 68Ga-HER2-Nanobody for PET/CT Assessment of HER2 Expression in Breast Carcinoma. *J Nucl Med* **2016,** *57*, (1), 27-33.
13. Kruwel, T.; Nevoltris, D.; Bode, J.; Dullin, C.; Baty, D.; Chames, P.; Alves, F. In vivo detection of small tumour lesions by multi-pinhole SPECT applying a (99m)Tc-labelled nanobody targeting the Epidermal Growth Factor Receptor. *Sci Rep* **2016,** *6*, 21834.
14. Van Audenhove, I.; Gettemans, J. Nanobodies as Versatile Tools to Understand, Diagnose, Visualize and Treat Cancer. *EBioMedicine* **2016,** *8*, 40-8.
15. Ren, Y. R.; Patel, K.; Paun, B. C.; Kern, S. E. Structural analysis of the cancer-specific promoter in mesothelin and in other genes overexpressed in cancers. *J Biol Chem* **2011,** *286*, (14), 11960-9.
16. Hassan, R.; Thomas, A.; Alewine, C.; Le, D. T.; Jaffee, E. M.; Pastan, I. Mesothelin Immunotherapy for Cancer: Ready for Prime Time? *J Clin Oncol* **2016,** *34*, (34), 4171-4179.
17. Prantner, A. M.; Turini, M.; Kerfelec, B.; Joshi, S.; Baty, D.; Chames, P.; Scholler, N. Anti-Mesothelin Nanobodies for Both Conventional and Nanoparticle-Based Biomedical Applications. *J Biomed Nanotechnol* **2015,** *11*, (7), 1201-12.
18. Scholler, N.; Garvik, B.; Quarles, T.; Jiang, S.; Urban, N. Method for generation of in vivo biotinylated recombinant antibodies by yeast mating. *J Immunol Methods* **2006,** *317*, (1-2), 132-43.
19. Bergan, L.; Gross, J. A.; Nevin, B.; Urban, N.; Scholler, N. Development and in vitro validation of anti-mesothelin biobodies that prevent CA125/Mesothelin-dependent cell attachment. *Cancer Lett* **2007,** *255*, (2), 263-74.
20. Roby, K. F.; Taylor, C. C.; Sweetwood, J. P.; Cheng, Y.; Pace, J. L.; Tawfik, O.; Persons, D. L.; Smith, P. G.; Terranova, P. F. Development of a syngeneic mouse model for events related to ovarian cancer. *Carcinogenesis* **2000,** *21*, (4), 585-91.
21. Nunez-Cruz, S.; Connolly, D. C.; Scholler, N. An orthotopic model of serous ovarian cancer in immunocompetent mice for in vivo tumor imaging and monitoring of tumor immune responses. *J Vis Exp* **2010**, (45).
22. Wienken, C. J.; Baaske, P.; Rothbauer, U.; Braun, D.; Duhr, S. Protein-binding assays in biological liquids using microscale thermophoresis. *Nat Commun* **2010,** *1*, 100.
23. Kelly, R. J.; Sharon, E.; Pastan, I.; Hassan, R. Mesothelin-targeted agents in clinical trials and in preclinical development. *Mol Cancer Ther* **2012,** *11*, (3), 517-25.
24. Morello, A.; Sadelain, M.; Adusumilli, P. S. Mesothelin-Targeted CARs: Driving T Cells to Solid Tumors. *Cancer Discov* **2016,** *6*, (2), 133-46.
25. Kobayashi, K.; Sasaki, T.; Takenaka, F.; Yakushiji, H.; Fujii, Y.; Kishi, Y.; Kita, S.; Shen, L.; Kumon, H.; Matsuura, E. A novel PET imaging using (6)(4)Cu-labeled monoclonal antibody against mesothelin commonly expressed on cancer cells. *J Immunol Res* **2015,** *2015*, 268172.

26. Lamberts, L. E.; Menke-van der Houven van Oordt, C. W.; ter Weele, E. J.; Bensch, F.; Smeenk, M. M.; Voortman, J.; Hoekstra, O. S.; Williams, S. P.; Fine, B. M.; Maslyar, D.; de Jong, J. R.; Gietema, J. A.; Schroder, C. P.; Bongaerts, A. H.; Lub-de Hooge, M. N.; Verheul, H. M.; Sanabria Bohorquez, S. M.; Glaudemans, A. W.; de Vries, E. G. ImmunoPET with Anti-Mesothelin Antibody in Patients with Pancreatic and Ovarian Cancer before Anti-Mesothelin Antibody-Drug Conjugate Treatment. *Clin Cancer Res* **2016,** *22*, (7), 1642-52.
27. Lindenberg, L.; Thomas, A.; Adler, S.; Mena, E.; Kurdziel, K.; Maltzman, J.; Wallin, B.; Hoffman, K.; Pastan, I.; Paik, C. H.; Choyke, P.; Hassan, R. Safety and biodistribution of 111In-amatuximab in patients with mesothelin expressing cancers using single photon emission computed tomography-computed tomography (SPECT-CT) imaging. *Oncotarget* **2015,** *6*, (6), 4496-504.
28. ter Weele, E. J.; Terwisscha van Scheltinga, A. G.; Kosterink, J. G.; Pot, L.; Vedelaar, S. R.; Lamberts, L. E.; Williams, S. P.; Lub-de Hooge, M. N.; de Vries, E. G. Imaging the distribution of an antibody-drug conjugate constituent targeting mesothelin with (8)(9)Zr and IRDye 800CW in mice bearing human pancreatic tumor xenografts. *Oncotarget* **2015,** *6*, (39), 42081-90.
29. De Vos, J.; Devoogdt, N.; Lahoutte, T.; Muyldermans, S. Camelid single-domain antibody-fragment engineering for (pre)clinical in vivo molecular imaging applications: adjusting the bullet to its target. *Expert Opin Biol Ther* **2013,** *13*, (8), 1149-60.
30. Kaneko, O.; Gong, L.; Zhang, J.; Hansen, J. K.; Hassan, R.; Lee, B.; Ho, M. A binding domain on mesothelin for CA125/MUC16. *J Biol Chem* **2009,** *284*, (6), 3739-49.
31. Ma, J.; Tang, W. K.; Esser, L.; Pastan, I.; Xia, D. Recognition of mesothelin by the therapeutic antibody MORAb-009: structural and mechanistic insights. *J Biol Chem* **2012,** *287*, (40), 33123-31.
32. Rump, A.; Morikawa, Y.; Tanaka, M.; Minami, S.; Umesaki, N.; Takeuchi, M.; Miyajima, A. Binding of ovarian cancer antigen CA125/MUC16 to mesothelin mediates cell adhesion. *J Biol Chem* **2004,** *279*, (10), 9190-8.
33. Scholler, N.; Garvik, B.; Hayden-Ledbetter, M.; Kline, T.; Urban, N. Development of a CA125-mesothelin cell adhesion assay as a screening tool for biologics discovery. *Cancer Lett* **2007,** *247*, (1), 130-6.
34. Sathyanarayana, B. K.; Hahn, Y.; Patankar, M. S.; Pastan, I.; Lee, B. Mesothelin, Stereocilin, and Otoancorin are predicted to have superhelical structures with ARM-type repeats. *BMC Struct Biol* **2009,** *9*, 1.
35. Gainkam, L. O.; Huang, L.; Caveliers, V.; Keyaerts, M.; Hernot, S.; Vaneycken, I.; Vanhove, C.; Revets, H.; De Baetselier, P.; Lahoutte, T. Comparison of the biodistribution and tumor targeting of two 99mTc-labeled anti-EGFR nanobodies in mice, using pinhole SPECT/micro-CT. *J Nucl Med* **2008,** *49*, (5), 788-95.
36. Huang, L.; Gainkam, L. O.; Caveliers, V.; Vanhove, C.; Keyaerts, M.; De Baetselier, P.; Bossuyt, A.; Revets, H.; Lahoutte, T. SPECT imaging with 99mTc-labeled EGFR-specific nanobody for in vivo monitoring of EGFR expression. *Mol Imaging Biol* **2008,** *10*, (3), 167-75.
37. Vaneycken, I.; Govaert, J.; Vincke, C.; Caveliers, V.; Lahoutte, T.; De Baetselier, P.; Raes, G.; Bossuyt, A.; Muyldermans, S.; Devoogdt, N. In vitro analysis and in vivo tumor targeting of a humanized, grafted nanobody in mice using pinhole SPECT/micro-CT. *J Nucl Med* **2010,** *51*, (7), 1099-106.

38. Mejias, M. P.; Hiriart, Y.; Lauche, C.; Fernandez-Brando, R. J.; Pardo, R.; Bruballa, A.; Ramos, M. V.; Goldbaum, F. A.; Palermo, M. S.; Zylberman, V. Development of camelid single chain antibodies against Shiga toxin type 2 (Stx2) with therapeutic potential against Hemolytic Uremic Syndrome (HUS). *Sci Rep* **2016,** *6*, 24913.

39. Weiner, L. M.; Adams, G. P. New approaches to antibody therapy. *Oncogene* **2000,** *19*, (53), 6144-51.

40. Yokota, T.; Milenic, D. E.; Whitlow, M.; Schlom, J. Rapid tumor penetration of a single-chain Fv and comparison with other immunoglobulin forms. *Cancer Res* **1992,** *52*, (12), 3402-8.

41. Jain, R. K. Physiological barriers to delivery of monoclonal antibodies and other macromolecules in tumors. *Cancer Res* **1990,** *50*, (3 Suppl), 814s-819s.

42. Juweid, M.; Neumann, R.; Paik, C.; Perez-Bacete, M. J.; Sato, J.; van Osdol, W.; Weinstein, J. N. Micropharmacology of monoclonal antibodies in solid tumors: direct experimental evidence for a binding site barrier. *Cancer Res* **1992,** *52*, (19), 5144-53.

43. Saga, T.; Neumann, R. D.; Heya, T.; Sato, J.; Kinuya, S.; Le, N.; Paik, C. H.; Weinstein, J. N. Targeting cancer micrometastases with monoclonal antibodies: a binding-site barrier. *Proc Natl Acad Sci U S A* **1995,** *92*, (19), 8999-9003.

44. Kwok, H. F.; Botkjaer, K. A.; Tape, C. J.; Huang, Y.; McCafferty, J.; Murphy, G. Development of a 'mouse and human cross-reactive' affinity-matured exosite inhibitory human antibody specific to TACE (ADAM17) for cancer immunotherapy. *Protein Eng Des Sel* **2014,** *27*, (6), 179-90.

45. Pegram, M.; Ngo, D. Application and potential limitations of animal models utilized in the development of trastuzumab (Herceptin): a case study. *Adv Drug Deliv Rev* **2006,** *58*, (5-6), 723-34.

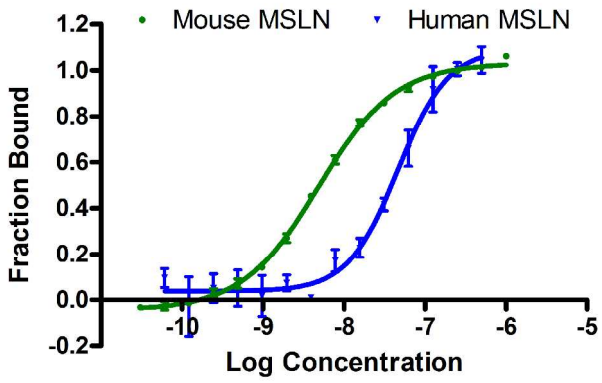

Figure 1. Microscale thermophoresis binding curves of anti-mesothelin nanobody G3a (NbG3a) to recombinant mouse and human mesothelin proteins. Equilibrium binding constants were of 4.8 ± 0.2 for mouse mesothelin protein and 46 ± 8 nM for human mesothelin protein. Points are the average and standard deviation from triplicate measurements.

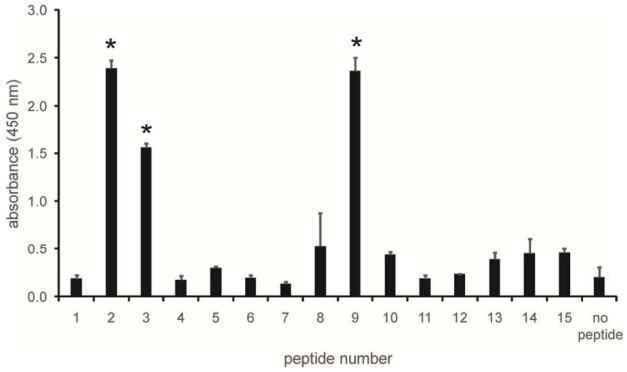

Figure 2. Epitope localization using an overlapping peptide array of human mesothelin. The binding of anti-mesothelin bNbG3a to 25-mer peptides with a 5-mer overlap was determined by ELISA. There is statistically significant (*: $p < 0.05$) specific recognition of peptides 2, 3, and 9. Background absorbance was determined with wells that were not coated with any peptide (no peptide).

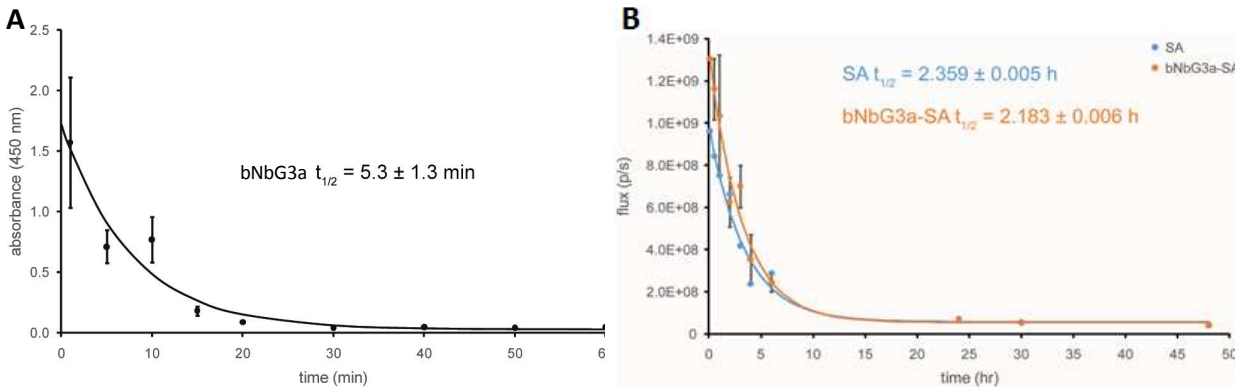

Figure 3. Pharmacokinetic analysis of bNbG3a alone or coupled to IRDye 680RD streptavidin. **A**. Blood samples were harvested 1 min, 5 min, 10 min, 15 min, 20 min, 30 min, 40 min, 50 min, 60 min, or 90 min after one intravenous injection of bNbG3a (30 μg), as indicated. The concentration of bNbG3a in serum was determined with an ELISA assay using anti-Flag antibody as capture and anti-V5-HRP antibody as detection. The half life was estimated using a one phase decay equation. Error bars when not visible are smaller than the symbols. **B**- Blood samples were harvested 5 min, 30 min, 1 hr, 2 hr, 3 hr, 4 hr, 6 hr, 24 hr, 30 hr or 48 hr after one intravenous injection of 30 μg of bNbG3a coupled to IRDye 680RD streptavidin (**orange line**) or of IRDye 680RD streptavidin only (**blue line**), as indicated. Sera were diluted 1/10 in PBS, imaged for fluorescent by In Vivo Imaging System (IVIS, PerkinElmer), and analyzed by Living Image software as radiant efficiency. Fluorescent data were plotted as shown to calculate the half-life of bNbG3a coupled to IRDye 680RD streptavidin (2.2 hrs) and of IRDye 680RD streptavidin only (2.3 hrs).

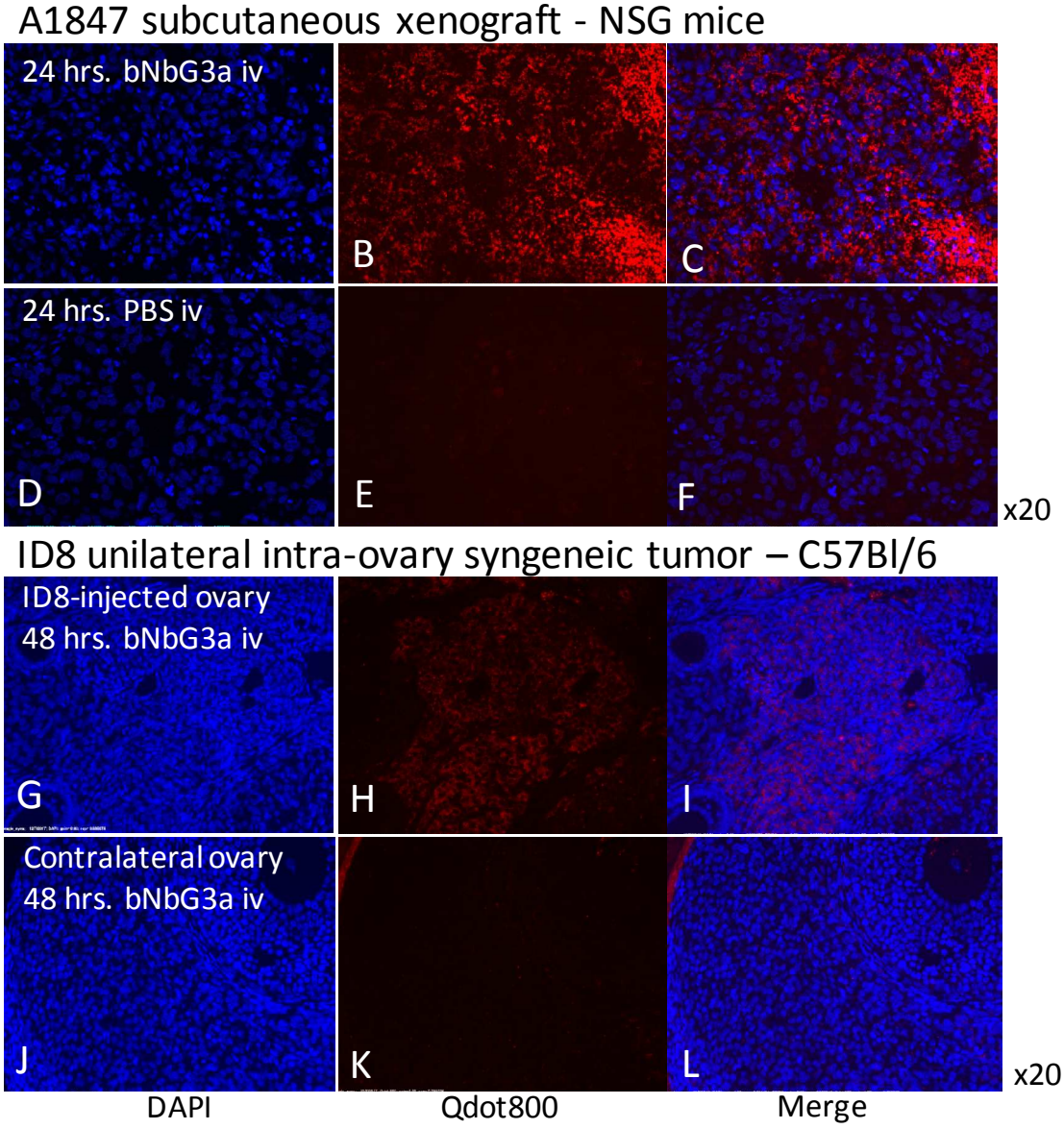

Figure 4. bNBG3a localizes in mesothelin-expressing xenograft and syngeneic tumor 24 hours after intra-venous injection. NSG mice were injected subcutaneously with human A1847 ovarian cancer cell line (**A-F**) and wild type C56Bl/6 mice were injected in the left ovary with ID8 mouse ovarian cancer cell line (**G-I**). The right ovary was left untouched (**J-L**). Six weeks later, mice were injected intravenously (iv) with 30 μg of bNbG3a (**A-C, G-L**) or with PBS (**D-F**) and sacrificed 24 hours (A1847, **A-F**) or 48 hours (**ID8, G-L**) later. Subcutaneous tumors,

ovarian tumors, and untouched ovaries were harvested, fixed, cut, mounted on glass slides, and stained with DAPI and Qdot800-labeled streptavidin. **Left panels**: DAPI staining. **Middle panels**: Qdot800-labeled streptavidin staining. **Right panels**: both stains. Images were taken using a 20x objective. Results representative of more than 2 independent experiments.

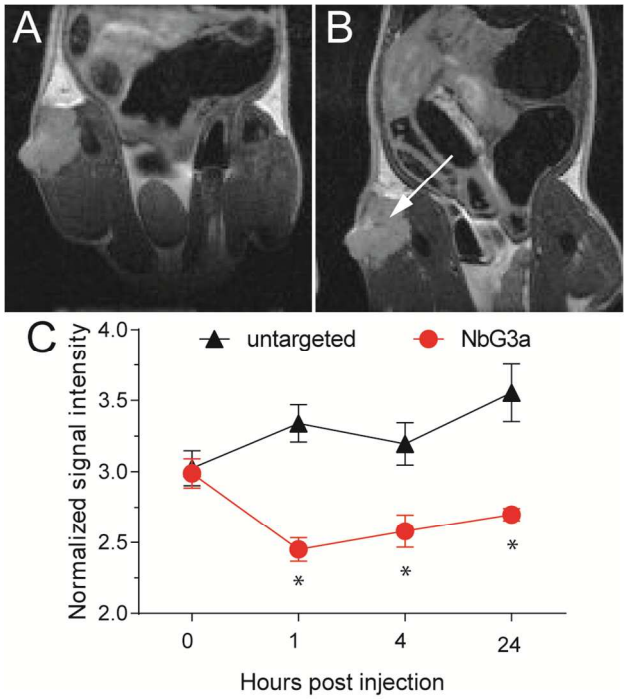

Figure 5. MRI imaging of a human ovarian cancer xenograft with bNbG3a. A-B: Representatives MRI image of a subcutaneous A1847 human ovarian cancer xenograft, seven weeks after tumor initiation before (**A**) and four hours after (**B**) injection with bNbG3a-targeted streptavidin-coated superparamagnetic nanoparticles. **C**- Mice were injected with either untargeted or bNbG3a-targeted streptavidin-coated superparamagnetic nanoparticles. Signal intensity of the tumor normalized to muscle signal intensity at the indicated time points was determined with a region-of-interest analysis using ImageJ (*: $p < 0.05$). The arrow in (**B**) indicates areas of signal reduction due to nanoparticle accumulation within the tumor.

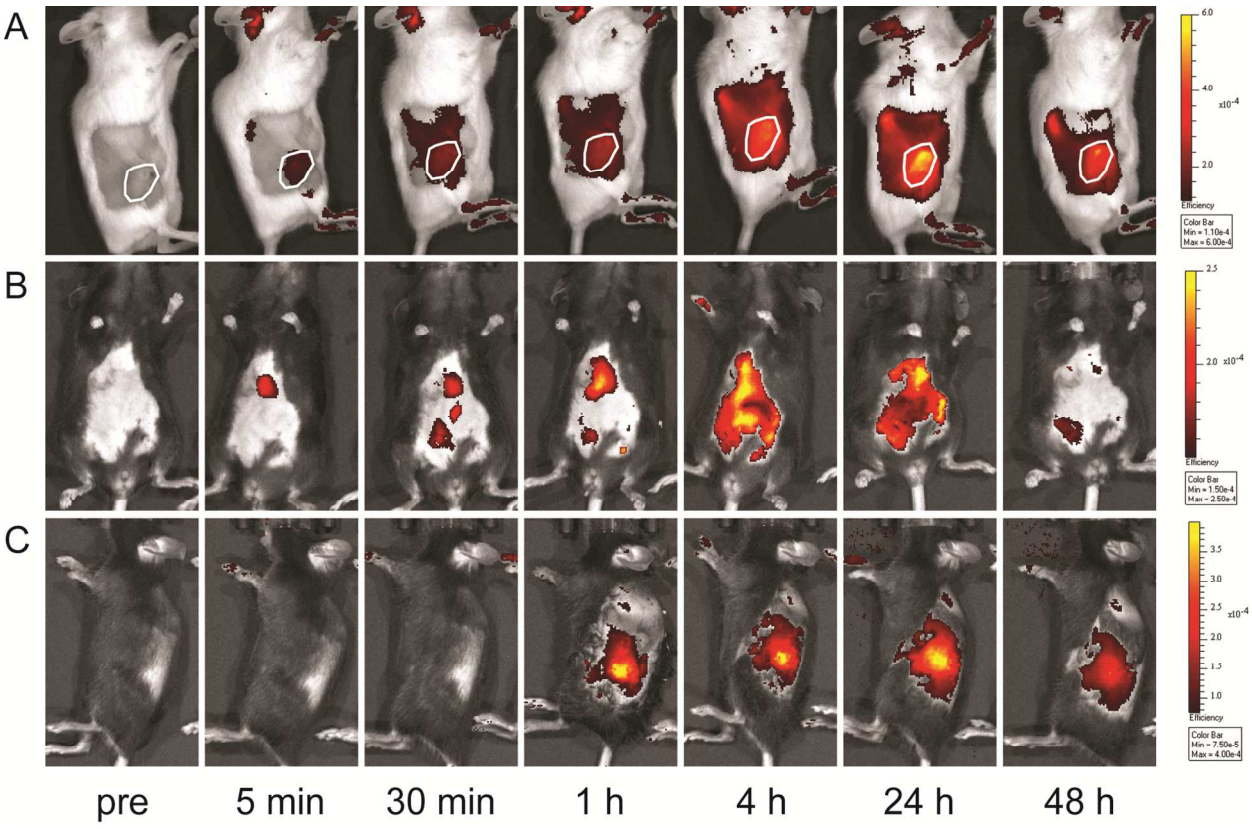

Figure 6. Optical imaging of ovarian tumor-bearing mice. The kinetics of tumor binding for bNbG3a coupled to IRDye 680RD streptavidin was determined in (**A**) a human A1847 xenograft or orthotopic Luc-ID8 models of (**B**) peritoneal and (**C**) intraovary tumors. Uptake kinetics differed between the mouse models, but all mice showed tumor fluorescence by 1 hour after an intravascular injection that remained until at least 24 hours post injection. Subcutaneous tumors are highlighted with a white polygon.

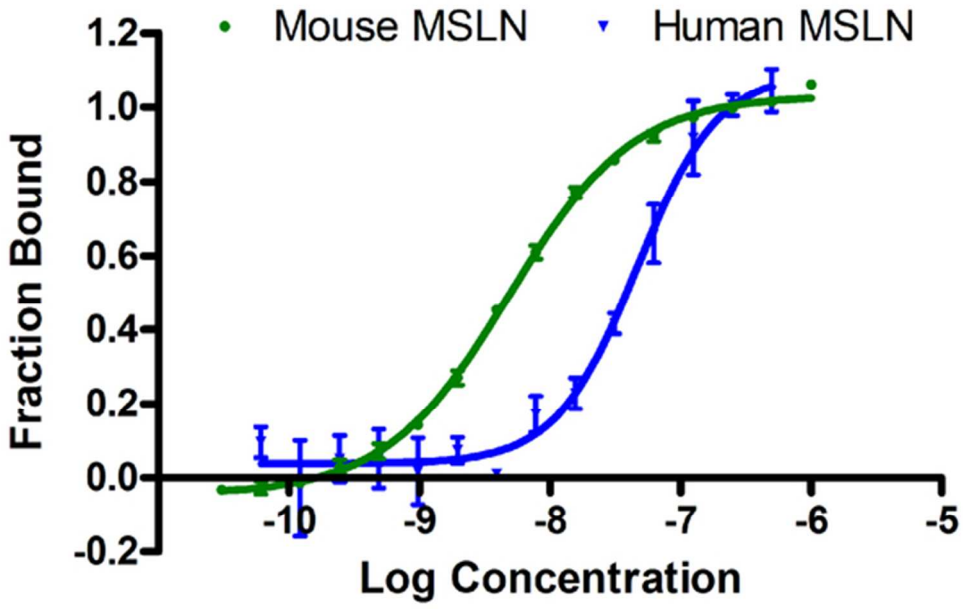

Figure 1. Microscale thermophoresis binding curves of anti-mesothelin nanobody G3a (NbG3a) to recombinant mouse and human mesothelin proteins. Equilibrium binding constants were of 4.8 ± 0.2 for mouse mesothelin protein and 46 ± 8 nM for human mesothelin protein. Points are the average and standard deviation from triplicate measurements.

52x33mm (300 x 300 DPI)

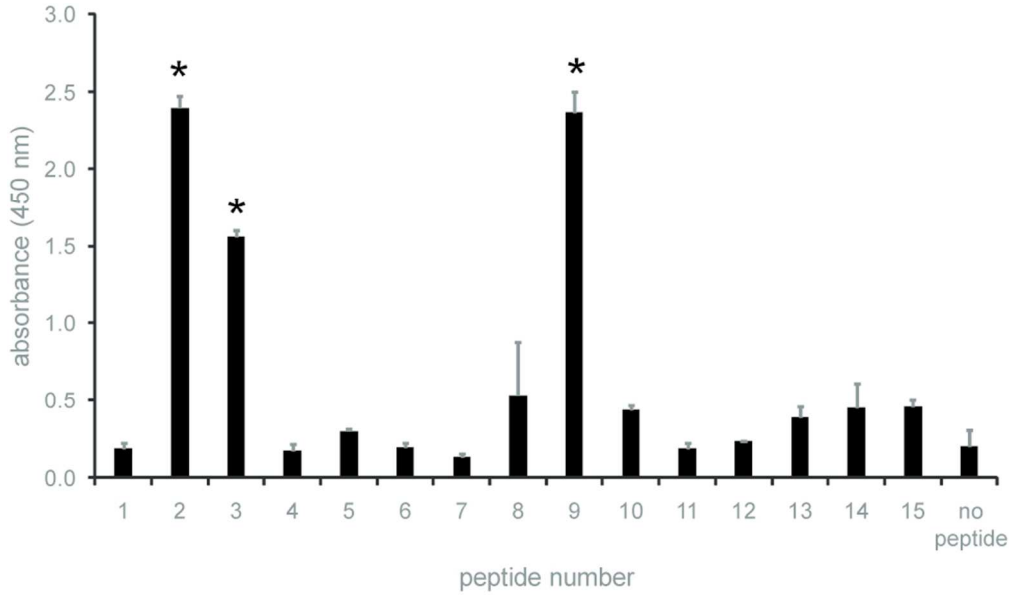

Figure 2. Epitope localization using an overlapping peptide array of human mesothelin. The binding of anti-mesothelin bNbG3a to 25-mer peptides with a 5-mer overlap was determined by ELISA. There is statistically significant (*: $p < 0.05$) specific recognition of peptides 2, 3, and 9. Background absorbance was determined with wells that were not coated with any peptide (no peptide).

81x48mm (300 x 300 DPI)

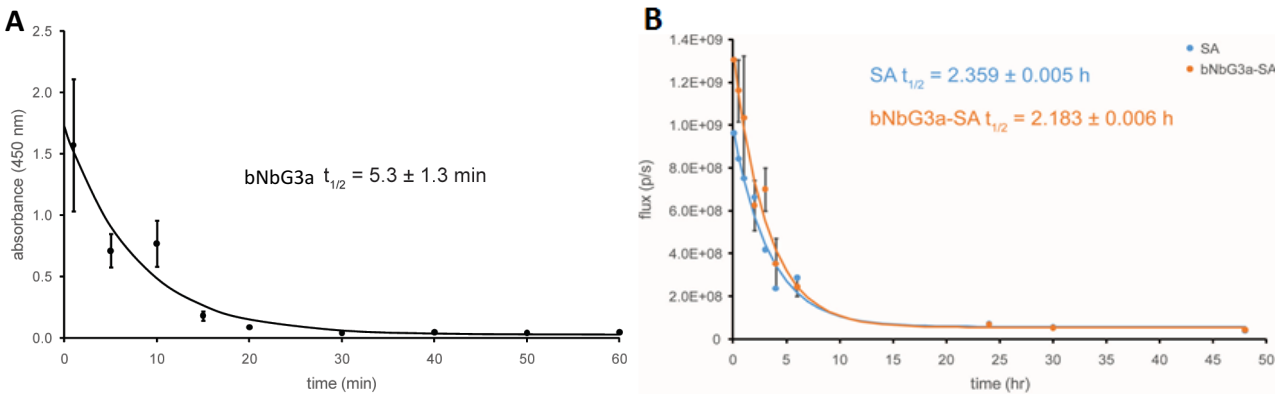
A
absorbance (450 nm)
time (min)
bNbG3a $t_{1/2}$ = 5.3 ± 1.3 min
B
flux (p/s)
time (hr)
SA $t_{1/2}$ = 2.359 ± 0.005 h
bNbG3a-SA $t_{1/2}$ = 2.183 ± 0.006 h
SA
bNbG3a-SA

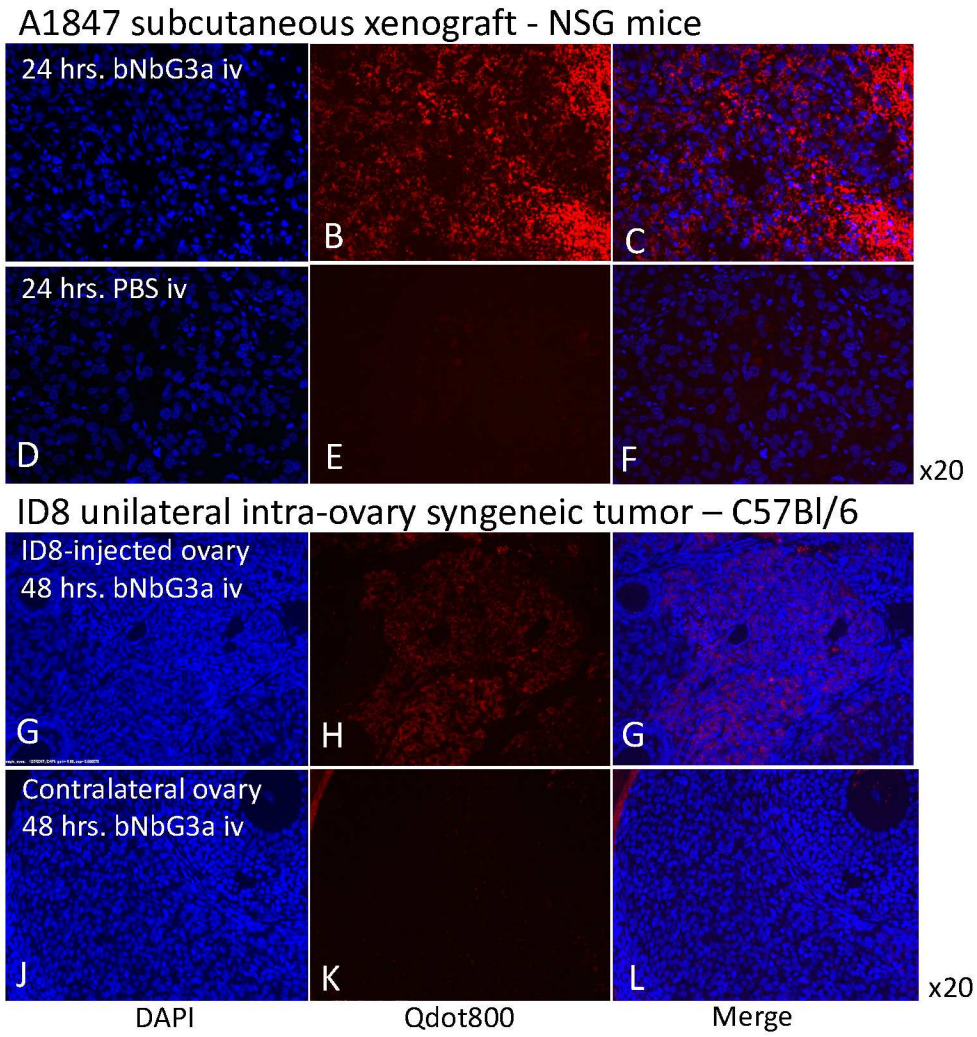
A1847 subcutaneous xenograft - NSG mice
24 hrs. bNbG3a iv
B
C
24 hrs. PBS iv
D
E
F
x20
ID8 unilateral intra-ovary syngeneic tumor – C57Bl/6
ID8-injected ovary
48 hrs. bNbG3a iv
G
H
G
Contralateral ovary
48 hrs. bNbG3a iv
J
K
L
x20
DAPI
Qdot800
Merge

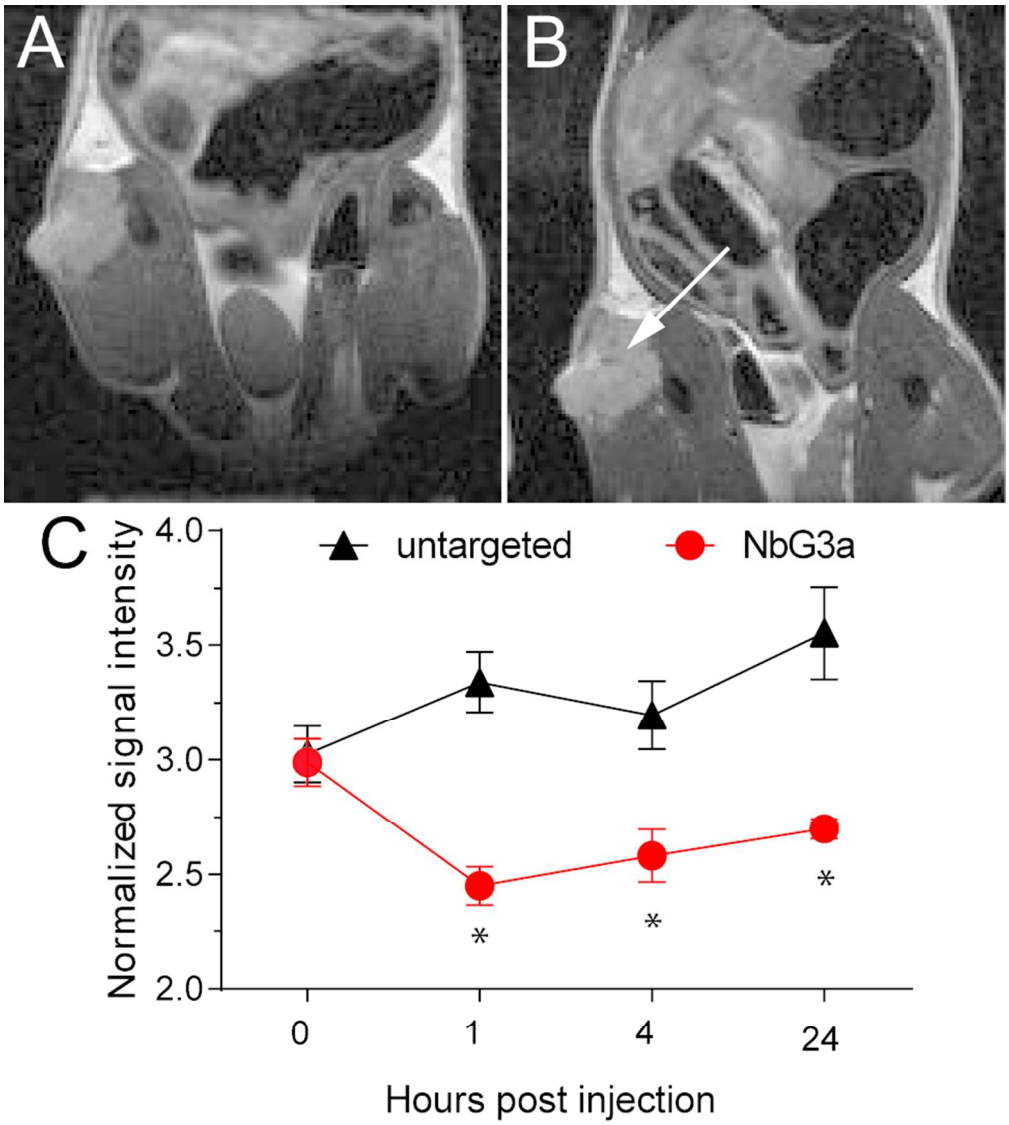

Figure 5. MRI imaging of a human ovarian cancer xenograft with bNbG3a. A-B: Representatives MRI image of a subcutaneous A1847 human ovarian cancer xenograft, seven weeks after tumor initiation before (A) and four hours after (B) injection with bNbG3a-targeted streptavidin-coated superparamagnetic nanoparticles. C- Mice were injected with either untargeted or bNbG3a-targeted streptavidin-coated superparamagnetic nanoparticles. Signal intensity of the tumor normalized to muscle signal intensity at the indicated time points was determined with a region-of-interest analysis using ImageJ (*: $p < 0.05$). The arrow in (B) indicates areas of signal reduction due to nanoparticle accumulation within the tumor.

81x91mm (300 x 300 DPI)

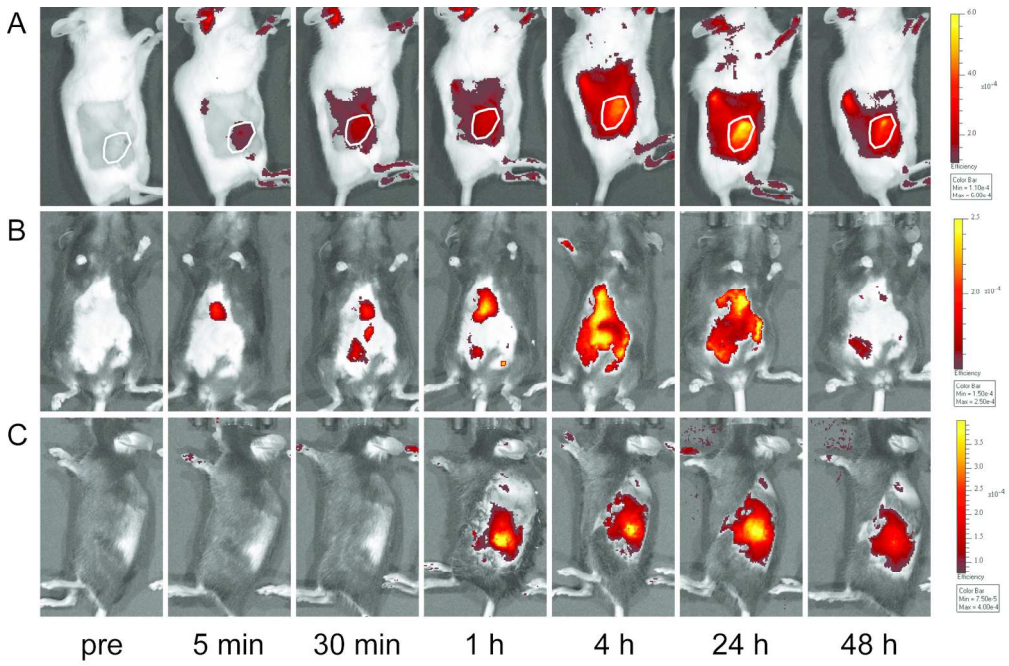

Figure 6. Optical imaging of ovarian tumor-bearing mice. The kinetics of tumor binding for bNbG3a coupled to IRDye 680RD streptavidin was determined in (A) a human A1847 xenograft or orthotopic Luc-ID8 models of (B) peritoneal and (C) intraovary tumors. Uptake kinetics differed between the mouse models, but all mice showed tumor fluorescence by 1 hour after an intravascular injection that remained until at least 24 hours post injection. Subcutaneous tumors are highlighted with a white polygon.

169x111mm (300 x 300 DPI)

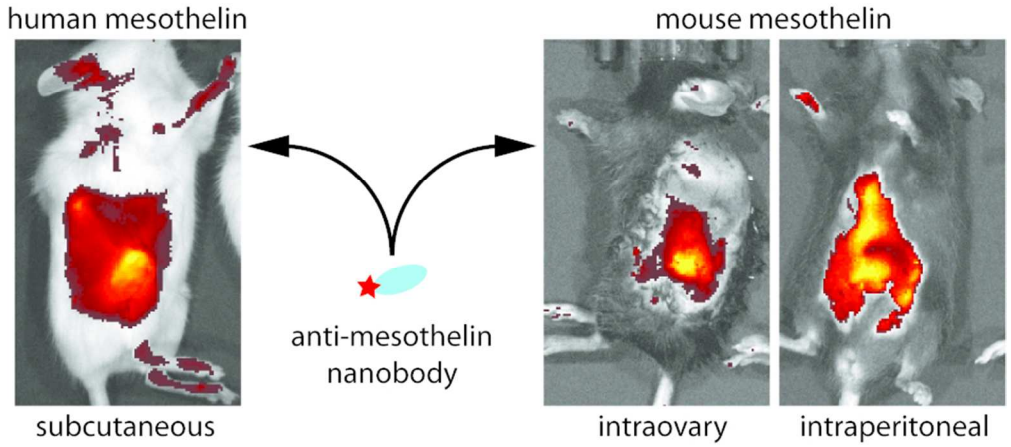

TOC graphic

80x35mm (300 x 300 DPI)